

Feb. 16

Near-Infrared Colors of Hard X-ray Selected Active Galactic Nuclei¹

Chisato Watanabe ²

Department of Astronomy, Kyoto University, Kyoto, 606-8502, Japan

`chisato@kusastro.kyoto-u.ac.jp`

Kouji Ohta ³

Department of Astronomy, Kyoto University, Kyoto, 606-8502, Japan

`ohta@kusastro.kyoto-u.ac.jp`

Masayuki Akiyama ^{2,3}

Subaru Telescope, National Astronomical Observatory of Japan, Hilo, HI, 96720

`akiyama@subaru.naoj.org`

and

Yoshihiro Ueda

Institute of Space and Astronautical Science, Sagami-hara, Kanagawa, 229-8510, Japan

`ueda@astro.isas.ac.jp`

ABSTRACT

¹Based on observations made with the Kitt Peak National Observatory 2.1m telescope, which is operated by National Optical Astronomy Observatories (NOAO) operated by AURA, Inc., under contract with the National Science Foundation and with the University of Hawaii 88 Inch telescope.

²Visiting Astronomer, University of Hawaii Observatory.

³Visiting Astronomer, Kitt Peak National Observatory, National Optical Astronomy Observatories (NOAO).

We present results of near-infrared photometry (J , H , K_S) for a hard X-ray selected sample of active galactic nuclei (AGNs) obtained from optical identification of the sources detected in *ASCA* surveys (total ~ 75 deg²) with a flux limit of $(1 - 3) \times 10^{-13}$ erg s⁻¹ cm⁻² (2–10 keV). The sample covers the AGNs at $0.1 \lesssim z \lesssim 1$ with $L_{2-10\text{keV}} \sim 10^{42} - 10^{46}$ erg s⁻¹ with very high completeness. The near-infrared photometric data of the sample are obtained from the Two Micron All Sky Survey (2MASS) and observations with Kitt Peak National Observatory 2.1 m telescope and the University of Hawaii 88 inch telescope. The fraction of red ($J - K_S > 2$ mag) AGNs in our sample is $\sim 2 \pm 1\%$, which is comparable to that for optically- or UV-selected quasi-stellar objects (QSOs, i.e. luminous AGNs). The number of red AGNs found in our sample is consistent with that expected from the surface density of red AGNs found in 2MASS by Cutri et al. (2001). We find that the anomalously-small dust-to-gas ratios in circumnuclear gas, which is seen in some AGNs with Seyfert-class luminosity, also occur in the QSOs (AGNs with luminosity of $L_{2-10\text{keV}} \geq 10^{44.5}$ erg s⁻¹) in the systematically surveyed sample in hard X-rays. For all the QSOs with an X-ray absorption of $N_{\text{H}} \geq 10^{22}$ cm⁻² in our sample, the values of A_V/N_{H} are smaller than the Galactic value by a factor of ~ 5 to ~ 100 . Since a fraction of this population among the QSOs in our sample is about 30%, such fraction of optical/UV-selected type 1 QSOs known to date may show type 2 nature in X-ray.

Subject headings: galaxies:active — surveys — quasars:general — X-rays:galaxies

1. Introduction

Many candidates of red, presumably moderately absorbed, quasi-stellar objects (QSOs) — luminous active galactic nuclei (AGNs) — have recently been found in QSO surveys in radio, X-ray, and near-infrared (NIR) wavelengths. Webster et al. (1995) revealed the presence of many red QSOs among radio-selected QSOs and suggested that the red color originated in an absorption to its nucleus. Since a significant fraction of the radio-selected QSOs has redder colors than optically-selected QSOs ($B - K = 2 \sim 3$ mag), it is argued that 80% of QSO population could be significantly absorbed and escape from traditional optical/UV selections. Subsequent studies revealed that the origin of the red color is not absorption to its nucleus, but a red synchrotron continuum of a jet component in $\sim 80\%$ of the red radio-loud QSOs (Francis et al. 2001). However, it is still possible that there is a large population of moderately ($E(B - V) \lesssim 1$ mag) reddened QSOs in radio-selected QSOs (White et al. 2003).

On the other hand, for radio-quiet QSOs, which are the dominant population of QSOs in the optical and X-ray wavelengths, the existence of red broad-line QSOs is reported in identification of soft X-ray selected *ROSAT* sources (Kim & Elvis 1999). Since the QSOs have harder X-ray spectra than optically-selected QSOs and have large $H\alpha$ to $H\beta$ broad-line flux ratios, it is likely that the extinction of $A_V \sim 2$ mag towards the nucleus makes the colors of the QSOs redder than optically-selected QSOs. The fraction of the red ($B - R > 2$ mag) QSO is not large ($\sim 1\% - 7\%$) in the soft X-ray selected sample, but a number of absorbed QSOs could be equal to that of the blue optically-selected QSOs (Kim & Elvis 1999), because the soft X-ray selection is biased to less absorbed QSOs and heavily absorbed QSOs are hard to be detected in the soft X-ray band. More recently, in the NIR wavelength, Two Micron All Sky Survey (2MASS) also has revealed the presence of many AGNs with NIR colors redder than $J - K_S = 2$ mag at $z \lesssim 0.3$ (2MASS red AGNs). The number density of the red AGNs is claimed to be comparable to that of optically-selected AGNs with $K_S < 14.5$ mag (Cutri et al. 2001, 2002).

The discoveries of red AGN population suggest that we have been missing a significant fraction of AGNs in traditional optical/UV selections of AGNs due to the moderate absorption to the nucleus. However the fraction of the red absorbed AGNs in the entire AGN population is not clear. Radio-selected samples are affected by red QSOs with the red synchrotron component. The Soft X-ray selection is biased to less absorbed QSOs and thus not suitable to disclose the fraction of the absorbed QSOs. The 2MASS-selected red AGNs are limited in the low redshift universe, primary because of the effect of the K -correction on intrinsic NIR colors of QSOs. Using a hard X-ray selected sample is one of the best ways to examine it because the hard X-ray is less affected by absorption, although very recently Wilkes et al. (2002) and Risaliti et al. (2003) have shown the presence of X-ray faint QSOs.

Another important issue in terms of absorption to an active nucleus is anomaly of dust-to-gas ratio in a circumnuclear region. In some of AGNs, an extinction to a nucleus estimated in optical light is significantly smaller than that derived from X-ray spectrum (e.g., Simpson 1998; Akiyama et al. 2000a; Risaliti et al. 2001; Akiyama, Ueda, & Ohta 2002b; Willott et al. 2003). Since the former extinction is caused by dust, while the latter by gas phase metal, this suggests that a dust-to-gas ratio is much smaller than the standard value obtained in the Galaxy. Maiolino et al. (2001a) compiled Seyfert galaxies showing evidence for absorption in the X-ray and/or NIR/optical data from literature, and found that the A_V/N_H values of most of them are 10 to 100 times smaller than the Galactic value. They claim that the most likely interpretation of this is the depletion of small grains due to coagulation (Maiolino, Marconi, & Oliva 2001b), though there may be other possibilities such as dust depletion due to sublimation by AGN radiation, or a difference in locations of X-ray and optical absorbing matters (Weingartner & Murray 2002). In any cases, the anomaly in dust-to-gas ratio affects

not only on the understanding of physical conditions in a circumnuclear region, but also on the view of the unified scheme of AGNs; there may be a population that shows type 1 nature in optical/UV region but show type 2 nature in X-ray region. The sample by Maiolino et al. (2001a) is rather heterogeneous and limited to low luminosity AGNs ($< 10^{44.5}$ erg s $^{-1}$ in a 2–10 keV band). We intend to extend the luminosity range higher (QSO regime) using an unbiased systematic sample obtained through optical follow-up of hard-X-ray source surveys.

To make a sample of AGNs at a higher redshift with a larger luminosity without biasing to less absorbed objects, we constructed a highly complete hard X-ray selected AGN sample covering a large survey area. Using a 2–10 keV hard X-ray emission, we can detect AGNs with an absorption up to N_{H} of $10^{22.5} \sim 10^{23}$ cm $^{-2}$ with a negligible bias in the redshift range below ~ 1 . In fact, a *Beppo-SAX* hard X-ray survey found a red QSO (Vignali et al. 2000), and the presence of many red optical counterparts found in deep *Chandra* and/or *XMM-Newton* surveys (Hasinger et al. 2001) hints that there are many red AGNs. However, the optical identification of these samples is not complete so it has been difficult to draw conclusions about what fraction of all AGN that is absorbed.

In this paper, we present NIR colors of hard X-ray (2–10 keV) selected AGN samples obtained through optical identification of hard X-ray surveys with *ASCA*. The optical identification is fairly complete and the sample is suitable to estimate the fraction of red AGNs and the distribution of A_V/N_{H} values in QSOs at intermediate redshifts. Throughout this paper, we use cosmological parameters of $H_0 = 70$ km s $^{-1}$ Mpc $^{-1}$, $\Omega_m = 0.3$, and $\Omega_\Lambda = 0.7$.

2. Hard X-ray Selected Samples

We use two hard X-ray selected samples of AGNs. One is a sample from the *ASCA* Large Sky Survey (ALSS) and its optical identification. The ALSS is a contiguous (~ 5 deg 2) sky survey near the north Galactic pole made with *ASCA* during a period from 1993 and 1995 (Ueda et al. 1999a). 34 X-ray sources with a flux larger than $\sim 1 \times 10^{-13}$ erg s $^{-1}$ cm $^{-2}$ (2–10 keV) were found in this survey (significance level larger than 3.5σ in the 2–7 keV Solid-state Imaging Spectrometer (SIS) band). Optical follow-up spectroscopy was made and 33 sources were successfully identified (Akiyama et al. 2000a); they consist of 30 AGNs at redshifts of 0.03 to 1.7, two clusters of galaxies and a Galactic star (one remaining X-ray source is possibly a false source; see footnote of Ueda et al. (2003)). The second sample is from the *ASCA* Medium Sensitivity Survey (AMSS) and its optical identification. The AMSS is a serendipitous source survey with *ASCA*; *ASCA* pointing observation data taken during a period from 1993 and 1996 were gathered and more than 1300 sources (including target sources) were detected in the fields of views of the Gas Imaging Spectrometer (GIS)

(Ueda et al. 1999b, 2001). Akiyama et al. (2003) defined a complete flux-limited sample for optical follow-up by selecting sources in the northern sky with fluxes larger than 3×10^{-13} erg s $^{-1}$ cm $^{-2}$ detected with significance above 5.5σ in the 2–10 keV band (AMSSn sample; more detailed criteria are described by Akiyama et al. 2003). The AMSSn contains 87 objects in a total survey area of ~ 70 deg 2 . We have identified all but one of them; 78 sources are AGNs (including 3 BL Lac objects), 7 clusters and 1 Galactic star (Akiyama et al. 2003).

In total, 105 AGNs (excluding 3 BL Lac objects) are found in the ALSS and AMSSn. The combined *ASCA* sample is unique even in comparison with AGN samples from *Chandra* and *XMM-Newton* surveys, because it is the largest hard X-ray selected AGN sample at a relatively bright flux limit of 10^{-13} erg s $^{-1}$ cm $^{-2}$ (2–10 keV). Table 1 summarizes the observed 2–10 keV flux and the absorption-corrected luminosity in the rest-frame 2–10 keV band for each *ASCA* source. We also list the intrinsic photon index Γ and absorption column-density to the nucleus N_{H} (and their 1σ errors), which are used to calculate the flux and luminosity. The photon index or absorption is estimated as described by Ueda et al. (2003), who utilize the hardness ratio above and below 2 keV (or the 3-bin GIS spectrum plus 2-bin SIS spectrum for the ALSS; see Ueda et al. 1999a for details); $N_{\text{H}} = 0$ is assumed if the best-fit Γ is larger than 1.9 while $\Gamma = 1.9$ for the other case. For AGNs for which follow-up observations were made with *XMM-Newton* or *ASCA*, both Γ and N_{H} are determined through X-ray spectral fits. Note that these values listed in Table 1 are slightly different from those in Akiyama et al. (2000a, 2003), where $\Gamma = 1.7$ is adopted (also, the flux values in their plots are based on an unabsorbed power-law spectrum with a varying photon index). The difference does not affect on our overall discussion, however.

Figure 1 shows the 2–10 keV flux against redshift for the sample in the left panel, and the absorption corrected luminosity in the rest-frame 2–10 keV band against redshift in the right panel. Over-plotted solid circles, crosses, and open squares indicate the AGNs with a large X-ray to optical flux ratio ($\log f_{2-10 \text{ keV}}/f_R > +1$, i.e., optically-faint), the AGNs showing no significant broad H β emission line, and the AGNs with a large X-ray absorption (N_{H} larger than 10^{22} cm $^{-2}$), respectively. The X-ray luminosity in the 2–10 keV band of them ranges from $\sim 10^{43}$ erg s $^{-1}$ to $\sim 10^{46}$ erg s $^{-1}$, and the N_{H} ranges from ~ 0 to $\sim 10^{23}$ cm $^{-2}$. The hard X-ray luminosities of the sample are one to two orders of magnitudes larger than those of AGN samples obtained with *Chandra* and *XMM-Newton* at $z \lesssim 1$. Therefore, the *ASCA* sample provides a good sample to study the high-luminosity absorbed AGN population in the intermediate redshift universe.

3. NIR and Optical Photometric Data Sources

For the *ASCA* AGN sample, we made a cross-correlation with 2MASS Point Source Catalog (the second incremental data release). The 10σ detection limits for a point source are 15.8, 15.1 and 14.3 mag at J , H , and K_S band, respectively in the catalog. We searched a 2MASS source each for an optical counterpart of the *ASCA* AGN within a radius of $1''.2$, except for one diffuse object. We found NIR counterparts for about half of the sample in the 2MASS catalog.

In order to obtain NIR photometric data for the *ASCA* AGNs without 2MASS counterpart, J , H , and K_S imaging observations were made with Simultaneous Quad Infrared Imaging Device (SQIID) attached to the Kitt Peak National Observatory (KPNO) 2.1 m telescope during 4 nights from 2002 March 29 to April 1. The SQIID can produce images of the same field in J , H , K_S , and L bands simultaneously, with four 512×512 ALADDIN InSb arrays. One pixel corresponds to $0''.69$, giving a field of view of $\sim 5 \times 5$ arcmin². About 50 *ASCA* AGNs which did not have 2MASS counterparts at the time of the observing run were observed. We took 5 images of each target with small ($\sim 20''$) offsets. A total integration time was 300 sec to 3600 sec for each object depending on its faintness. A typical seeing size (FWHM) during the observations was $2''$ and the sky conditions were photometric.

The data were reduced using IRAF in the following manner. After correcting bad pixels by interpolating a pixel value from surrounding pixels, a dark frame was subtracted. Flat fielding was done with flat frames which were constructed by averaging the normalized object frames taken within a few hours in each band. A background sky was determined by a one-dimensional polynomial fitting to the flat-fielded frame and was removed. Using positions of bright stars (but not saturated) in a frame, five frames for each target with small offsets were combined to one frame by taking average.

Since the SQIID adopted the filter system very close to that of the 2MASS, a calibration of magnitude was made by using objects cataloged in 2MASS Point Source Catalog and not cataloged in 2MASS Extended Source Catalog (i.e., excluding extended sources in the point source catalog). About 100 stellar-objects in 23 target fields were used. We restricted the magnitude ranges of the objects for the calibration to avoid non-linearity and poor S/N; $12.5 \text{ mag} < J < 16.0 \text{ mag}$, $12.5 \text{ mag} < H < 15.5 \text{ mag}$, $12.5 \text{ mag} < K_S < 15.5 \text{ mag}$. By taking account of colors of the objects and air mass of each frame, we determined a zero-point in each band with 3σ clipping algorithm. The obtained zero-points are accurate with an uncertainty of $\pm 0.01 \text{ mag}$ for all the bands.

Photometry of the target objects was made as follows: First, we estimated a residual local-sky value with the median of pixel values in an annular region around the object (a 6

– 15 pixel radius with a 6 – 15 pixel width). Counts at the saturation radius of the growth curve of each target was adopted to be total counts. The photometric error for each object was estimated by measuring counts in an aperture with the same size for the target object randomly putting into the object frame. We put 10 apertures one time and repeated it 10 times for each object frame. Thus total 100 values were obtained for each target, and we assigned the rms value as the error of the target magnitude. Resulting magnitudes and errors are listed in Table 1.

About one year later after our observations, the 2MASS All-Sky Data Release was released. Among the targets observed with the KPNO 2.1 m, which were not cataloged in the 2nd Incremental Data Release, 23 sources were found in the All-Sky Catalog. The colors agree with each other, although a systematic error of ~ 0.1 mag may exist. Since the KPNO data have higher S/N than those of 2MASS, we adopt the KPNO data in this paper. The 2MASS All-Sky Data also provided us several new photometric data for our sample, of which NIR data had not been available.

Additional observations were made on 2003 June 14 and 15 with QUick InfraRed Camera (QUIRC) employing a 1024×1024 HgCdTe array attached to the University of Hawaii (UH) 88 Inch telescope; 9 of the remaining AGNs in the sample, for which no NIR photometric data were available or only poor-S/N data were obtained, were observed in J , H , and K' bands. The pixel scale of the camera was $0.''19$, giving a field of view of 3.2×3.2 arcmin² and the seeing size during the observations was typically $\sim 0.''8$. We took more than 4 images of each target in each band with small ($\sim 10''$) offsets. Total exposure time for each target ranged 5 min to 72 min depending on its faintness. During the observations, 4 UKIRT faint standard stars were observed for photometric calibration. All the data were reduced using IRAF in the same manner. Dark-frame subtraction, flat-fielding with self-flat frames, background subtraction, matching the seeings, and image stacking were performed. Errors on magnitudes of the targets were ~ 0.1 mag or less in all the bands. K' magnitudes were converted to K_S magnitudes by using the equations given by Wainscoat and Cowie (1992), UKIRT web site ¹, and Section VI.4.b of the 2MASS Explanatory Supplement ². In summary, we obtained NIR photometric data for 104 out of 105 of the *ASCA* AGNs. The results are presented in Table 1. (One object without NIR data in our sample is 1AXG J035008–1149 (SE37).)

Optical photometric data are mainly taken from the APM catalog (Irvin, Maddox, & McMahon 1994). The O and E magnitudes of APM catalog are converted to B and R

¹http://www.jach.hawaii.edu/JACpublic/UKIRT/astronomy/calib/phot_trans.html

²http://www.ipac.caltech.edu/2mass/releases/allsky/doc/sec6_4b.html

magnitudes by using the equations by Evans (1989). B and R magnitudes are obtained for $\sim 80\%$ and 100% of the sample objects, respectively, as shown in Table 1. Errors of B and R magnitudes are not available and we adopt 0.5 mag as a typical error. Supplemental optical magnitudes are taken from our own data (Akiyama et al. 2000a, 2003); they are noted in Table 1.

4. Results and Discussions

4.1. K_S magnitudes and Hard X-ray Flux

In Figure 2, K_S magnitude against 2–10 keV flux is shown for our sample with open circles. Over-plotted filled circles, crosses, and open squares are the same as those in Figure 1. A symbol size of an open circle represents the 2–10 keV luminosity; large, middle, and small symbols indicate the AGNs with the 2–10 keV luminosity larger than 10^{45} erg s $^{-1}$, 10^{44-45} erg s $^{-1}$, and smaller than 10^{44} erg s $^{-1}$, respectively. Dashed lines represent the constant X-ray to NIR flux ratio of $\log f_{2-10 \text{ keV}}/f_{K_S} = +3, +2, +1, 0, -1, -2$, and -3 , from top to bottom. Most of the *ASCA* AGNs distribute between $\log f_{2-10 \text{ keV}}/f_{K_S} = 0$ and $+1$, which is consistent with that of the mean spectrum of radio-quiet QSOs by Elvis et al. (1994) ($\log f_{2-10 \text{ keV}}/f_{K_S} \sim +0.4$). All but one of the optically-faint AGNs in the sample (shown with filled circles) fall above the line of $\log f_{2-10 \text{ keV}}/f_{K_S} = +1$. It is also notable that AGNs without broad H β emission lines (crosses), most of which are type 2 Seyferts at relatively lower redshift, tend to have relatively small X-ray to K_S flux ratios. If the AGN components of them have the same X-ray to K_S flux ratios as those of the other AGNs in our sample, the excess in K_S flux at a given X-ray flux is considered to be caused by the contribution of their host galaxy light.

4.2. Color Distribution of the Hard X-ray Selected Sample

The $J - K_S$ colors of the *ASCA* AGNs are plotted as a function of redshift in Figure 3. Over-plotted filled circles, crosses, and open squares are the same as those in Figure 1. Small dots represent the optically-selected QSOs; counterparts in 2MASS (Second Incremental Data Release) of QSOs in Veron-Cetty & Veron catalog (2000) excluding radio-loud QSOs (Barkhouse & Hall 2001). Solid, dotted, and dashed lines show color tracks for the mean-QSO spectrum by Elvis et al. (1994), for that with an absorption of $A_V = 1$ mag, and for a template spectrum of an Sbc galaxy by Coleman, Wu, & Weedman (1980) to represent the color of a host galaxy of an AGN, respectively. No evolution is considered. $B - K_S$ color

against redshift for the *ASCA* sample is plotted in Figure 4. Marks and tracks are the same as those in Figure 3.

In Figures 3 and 4, the *ASCA* AGNs distribute between the Sbc-galaxy and the mean-QSO color tracks or around them at $z \lesssim 0.3$, while at $z \gtrsim 0.3$, they locate around the mean-QSO color track. At the low redshift, most of the sample are low luminous AGNs (Seyfert class); the total colors are mixture of those of host galaxies and nuclei. The objects at the high redshift are mostly luminous AGNs, resulting in that their colors show those of ordinary QSOs.

Since almost all of the optically-selected QSOs have $J - K_S < 2.0$ mag, we adopt $J - K_S > 2.0$ mag as a criterion for red AGNs, which is the same as that adopted by Cutri et al. (2001). In our sample, two out of 104 AGNs show red color. Therefore, the fraction of the red AGNs in the *ASCA* sample is $2 \pm 1\%$. If the error bars of $J - K_S$ color for the sample AGNs are considered, the maximum of the fraction is $\sim 8 \pm 3\%$. Thus among the AGNs with the 2–10 keV flux larger than $\sim 10^{-13}$ erg s $^{-1}$ cm $^{-2}$, the fraction of red AGNs is not significantly larger than that in the optically-selected sample ($\sim 5\%$) (Barkhouse & Hall 2001).

On the other hand, the $B - K_S$ color distribution of the *ASCA* AGNs seems to be biased toward red compared with the optically-selected QSOs (dots) particularly at $z \lesssim 0.3$. Most of the *ASCA* AGNs showing red $B - K_S$ color are type 2 Seyferts, so the origin of their red color is likely to be host-galaxy light.

4.3. Individual Notes on Red AGNs in the *ASCA* Sample

There are only two AGNs with $J - K_S$ colors redder than 2 mag in our sample; 1AXG J121854+2957 (NO07) with $J - K_S = 2.98$ mag and 1AXG J172938+5230 (NO10) with $J - K_S = 2.03$ mag. There are six AGNs at $z > 0.6$ showing similarly red ($J - K_S \sim 2$ mag) colors, which are redder than those of the other AGNs in the redshift range. These 8 red AGNs are marked with over-plotted pluses in Figure 2. We discuss these objects and the origin of the red colors in this section. In each panel of Figure 5, the NIR and optical photometric data points of each red AGN are shown by filled and open squares with the error, respectively. Solid and dashed lines indicate the mean-QSO spectrum (Elvis et al. 1994) with the absorption shown in the figure (Galactic extinction curve by Cardelli, Clayton, & Mathis (1989) is used) and the Sbc-galaxy template (Coleman et al. 1980) without absorption, respectively. These model spectra are independently fitted to the NIR data points of each AGN with the least-square method. It should be noted that the optical

and NIR data are not coeval so that the variability may affect the spectral energy distribution (SED) for each AGN.

4.3.1. ASCA AGNs with $J - K_S > 2.0$ mag

1AXG J121854+2957 (NO07) has the reddest $J - K_S$ color (2.98 mag) among the sample. It is an AGN at $z = 0.178$ with an intrinsic (i.e., absorption corrected) X-ray luminosity of $L_{2-10 \text{ keV}} = 1.1 \times 10^{44} \text{ erg s}^{-1}$. The $H\beta$ emission line of this AGN is narrow, but the $H\alpha$ emission line has a faint wing (Fiore et al. 1999). Thus this object seems to be a Seyfert 1.9. The SED of the AGN from B to K_S is shown in Figure 5. The mean-QSO spectrum with $A_V = 4.5$ mag can well reproduce the SED from J to K_S . The A_V is considerably smaller than that expected from the X-ray absorption of this AGN; by using the Galactic dust-to-gas ratio of $A_V/N_H = 5.6 \times 10^{-22} \text{ mag cm}^2$ (Predehl & Schmitt 1995), $A_V = 46_{-4}^{+6}$ mag is estimated from the $N_H = 8.2_{-0.7}^{+1.1} \times 10^{22} \text{ cm}^{-2}$ derived from the X-ray spectrum of this AGN obtained with *XMM-Newton* (Loaring, Page, & Ramsay 2003). If the mean-QSO spectrum with $A_V = 4.5$ mag is assumed, B and R -band data show excesses; a contribution from the galaxy may brighten B and R -band magnitudes. It is consistent with a fact that this AGN appears to be nearly point-like in NIR images but extended in optical images. Although the NIR SED can be also reproduced by a galaxy spectrum with an absorption of $A_V = 8.4$ mag and with a luminosity of about $17 L^*$, it is unlikely because the host galaxy seems to be too bright. In Figure 2, this AGN locates near the line of $\log f_{2-10 \text{ keV}}/f_{K_S} = 0$, which is close to a location occupied by a part of the 2MASS red AGNs shown with filled triangles.

1AXG J172938+5230 (NO10) is a broad-line AGN at $z = 0.278$ with an intrinsic X-ray luminosity of $L_{2-10 \text{ keV}} = 1.7 \times 10^{44} \text{ erg s}^{-1}$. It looks like a point source on the NIR and optical images. Its SED from J to K_S is well reproduced with the mean-QSO spectrum with $A_V = 0.8$ mag, but in this case, B and R -band magnitudes are too bright. The mean-QSO spectrum without absorption can reproduce the optical and NIR SED reasonably well. It is consistent with the fact that the deviation of $J - K_S$ color from the mean-QSO track is small as seen in Figure 3. In Figure 2, this AGN also locates close to the line of $\log f_{2-10 \text{ keV}}/f_{K_S} = 0$.

4.3.2. ASCA AGNs with $J - K_S \sim 2.0$ mag at $z > 0.6$

1AXG J160118+0844 (NO53) is an AGN at $z = 0.606$ with an intrinsic X-ray luminosity of $L_{2-10 \text{ keV}} = 5.9 \times 10^{44} \text{ erg s}^{-1}$. Its X-ray luminosity and narrow $H\beta$ emission line suggest that it is a candidate of a type 2 QSO. It is an optical-faint, radio-loud (figure 15 of Akiyama et al.(2003)) AGN. In the optical and NIR images, it appears to be a point source. The SED of this AGN is roughly reproduced with the mean-QSO spectrum with an absorption of $A_V = 1.5$ mag, which is very much smaller than that estimated from the X-ray absorption ($N_H = 3.0^{+1.6}_{-1.2} \times 10^{22} \text{ cm}^{-2}$ corresponding to $A_V = 17^{+9}_{-7}$ mag). The SED can also be reproduced with a galaxy spectrum with an intrinsic luminosity of about $6 L^*$.

AX J131831+3341 (LSS228) is an AGN at $z = 0.653$ with an intrinsic X-ray luminosity of $L_{2-10 \text{ keV}} = 7.8 \times 10^{44} \text{ erg s}^{-1}$. Although its $H\beta$ emission line is narrow, it shows a broad emission line of Mg II λ 2800. The absorption derived from X-ray spectrum is $N_H = 1.1^{+0.4}_{-0.4} \times 10^{22} \text{ cm}^{-2}$. This object is an optical-faint object. The SED of this object is roughly consistent with the mean-QSO spectrum with $A_V = 1.1$ mag or the galaxy template with a luminosity of about $5 L^*$. However, its optical and NIR images show that it has a nuclear component and an extended component, and we need to discuss the SED for each component. Akiyama et al. (2000b) and Akiyama and Ohta (2001) discuss this in detail. Its nucleus is very red; $I - K = 4.29$ mag, which corresponds to the absorption of $A_V \sim 3$ mag for the power-law continuum of an index of $\alpha = -0.5$. The NIR and optical colors of the extended component are consistent with the post-starburst nature of the host galaxy.

1AXG J210738-0512 (NO17) is a broad-line AGN at $z = 0.841$ with an intrinsic X-ray luminosity of $L_{2-10 \text{ keV}} = 1.2 \times 10^{45} \text{ erg s}^{-1}$. It appears nearly a point source in the NIR image but a slight elongation may be seen in the optical image. This is an optical-faint, radio-loud object. Its NIR SED is consistent with the absorbed mean-QSO spectrum with $A_V = 1.3$ mag, which is very much smaller than that inferred from the X-ray absorption ($N_H = 4.3^{+2.1}_{-1.7} \times 10^{22} \text{ cm}^{-2}$ corresponding to $A_V = 24^{+12}_{-10}$ mag). The red NIR colors are also accountable with a galaxy with a luminosity of about $4 L^*$. However we prefer the former interpretation, because it has a large X-ray luminosity, shows the broad emission line, and has a point-like morphology.

AX J131021+3019 (LSS039) is a broad-line AGN at $z = 1.152$ ³ with an intrinsic X-ray luminosity of $L_{2-10 \text{ keV}} = 1.8 \times 10^{45} \text{ erg s}^{-1}$. The object is point like in the optical image, but there is a hint of the presence of an extended feature in the NIR images. Its NIR SED

³The identification of this X-ray source was not correct in Akiyama et al. (2000a). Subsequent *XMM-Newton* observation revealed that object Z by Akiyama et al. (2000a) is the correct identification (See also Ueda et al. 2003).

is reasonably reproduced with the mean-QSO spectrum with $A_V = 1.4$ mag or the galaxy spectrum with a luminosity of about $17 L^*$. Again we prefer the former interpretation with the same reasons as those for NO17.

1AXG J233200+1945 (NO18) is an AGN at $z = 1.416$ with an intrinsic X-ray luminosity of $L_{2-10 \text{ keV}} = 3.5 \times 10^{45} \text{ erg s}^{-1}$. There is a hint of a broad Mg II emission line. This is an optical-faint source. In the optical and NIR images, it appears to be a point source. The SED of the AGN is consistent with the mean-QSO spectrum with an absorption of $A_V = 1.0$ mag, which is nearly two orders of magnitude smaller than that estimated from the X-ray absorption ($N_H = 1.1^{+0.6}_{-0.5} \times 10^{23} \text{ cm}^{-2}$ corresponding to $A_V = 62^{+34}_{-28}$ mag). Although the galaxy spectrum with a luminosity of about $17 L^*$ can also reproduce the NIR SED, we favor the former interpretation with the same reasons as those for NO17.

1AXG J150423+1029 (NO04) is a broad-line AGN at $z = 1.839$ with an intrinsic X-ray luminosity of $L_{2-10 \text{ keV}} = 1.2 \times 10^{46} \text{ erg s}^{-1}$. It is an optical-faint object. It is a radio-loud, bright quasar. In the optical and NIR images, it appears to be a point source. Its SED is consistent with the mean-QSO spectrum with an absorption of $A_V = 1.2$ mag, which is smaller than that estimated from the X-ray absorption ($N_H = 5.4^{+1.8}_{-1.7} \times 10^{22} \text{ cm}^{-2}$ corresponding to $A_V = 30^{+10}_{-10}$ mag) by more than one order of magnitude. The SED is also consistent with the galaxy spectrum with a luminosity of about $1000 L^*$, which seems to be exceptionally bright. Therefore, we prefer the former interpretation.

In summary, the relatively-red colors in NIR band of these six AGNs at $z > 0.6$ are presumably originated from nuclear light with absorption of $A_V \sim 1 - 2$ mag or galaxy light with a luminosity of $\sim 4 - 17 L^*$. For many of these AGNs, we favor the former interpretation because of their point-like appearance, high luminosity in X-ray, and/or existence of a broad emission line. 5 out of 6 these AGNs have hard X-ray to K_S band flux ratios larger than $\log f_{2-10\text{keV}}/f_{K_S} = +1$. It suggests that these AGNs are different population from the 2MASS red AGNs, which have hard X-ray to K_S band flux ratios of $\log f_{2-10\text{keV}}/f_{K_S} \lesssim 0$.

4.4. Dust-to-Gas Ratios in QSOs

In this subsection, we estimate the dust-to-gas ratios of QSOs in the *ASCA* sample to investigate whether the anomalous dust-to-gas ratios found in low-luminous AGNs (Seyferts) are also seen in QSOs or not. In Figure 6, A_V/N_H values normalized to the Galactic one are plotted against 2–10 keV luminosity for the X-ray absorbed ($N_H \geq 10^{22} \text{ cm}^{-2}$) QSOs ($L_{2-10 \text{ keV}} \geq 10^{44.5} \text{ erg s}^{-1}$) among the *ASCA* sample. Open circles and open triangles show the radio-quiet and radio-loud QSOs of the sample, respectively. Over-plotted crosses

and filled circles are the same as those in Figure 1. The N_{H} is estimated from the X-ray spectrum as described in section 2, and the A_V is calculated from the observed $J - K_S$ color on the assumption that the intrinsic spectrum of a QSO is the same as that of the mean-QSO spectrum by Elvis et al. (1994). Since both X-ray and K_S luminosities are very high (the absolute K_S magnitudes of them are brighter than ~ -26 mag which is 1.5 mag brighter than M_K^* for local galaxies (Huang et al. 2003)), the contribution to NIR light from a host galaxy is assumed to be negligible. The uncertainty of A_V/N_{H} shown in the figure is calculated from the errors of $J - K_S$ color and of N_{H} for each QSO as well as the dispersion of distribution in $J - K_S$ color of the optically-selected QSOs. When no nominal optical absorption is obtained, an upper possible limit on A_V/N_{H} is calculated by considering the uncertainty, and is shown with an arrow.

Figure 6 shows that all the sample QSOs have A_V/N_{H} values smaller than the Galactic value by an order of magnitude or more⁴. This trend is the same as that seen in less luminous AGNs by Maiolino et al. (2001a), and it is indicated that the anomaly of the dust-to-gas ratio also occur in QSO-class AGNs. Furthermore, all the objects in Figure 6 show the presence of broad components at least in one of the emission lines of C IV λ 1549, Mg II λ 2800, H β , and H α , which also indicates the lack of the heavy extinction in the optical/UV region. The results show not only the existence of a population that has a type 1 nature in the optical/UV band but show a type 2 nature in the X-ray band, but also show that it is not a rare population. Since a fraction of this population in our sample is about 30% among the sample with the X-ray luminosity larger than $10^{44.5}$ erg s $^{-1}$, such fraction of optical/UV-selected type 1 QSOs known to date may have large amount of dust-less circumnuclear gases.

4.5. Comparison with 2MASS red AGNs

Cutri et al. (2001) revealed the presence of many red ($J - K_S > 2$ mag) AGNs at $z \lesssim 0.3$, by making optical follow-up for the red AGNs candidates selected with the 2MASS catalog (2MASS red AGNs). The optical follow-up spectroscopy of a part of them indicates that they are mixture of type 1 and type 2 AGNs; the number of type 2 is about one third of that of type 1. They claim that the number density of red type 1 AGNs is comparable to that of known QSOs selected in optical or UV.

⁴It should be noted that about half (4/10) of the sample QSOs are radio-loud. Since radio-loud QSOs tend to have flatter X-ray spectrum than radio-quiet ones, their N_{H} values derived by assuming an intrinsic power-law spectrum of photon index of 1.9 may be over-estimated. However, even if an intrinsic photon index of 1.7 is assumed, their N_{H} values are reduced by only 20% typically.

How many these red AGNs are predicted to be detected in our surveys with *ASCA* ? The total survey area of ALSS and AMSSn is $\sim 75 \text{ deg}^2$. Since the surface number density of red AGNs is $\sim 0.2 \text{ deg}^{-2}$ for $K_S \lesssim 14 \text{ mag}$ (Cutri et al. 2001), the region of our surveys should contain about 15 red AGNs with $K_S \lesssim 14 \text{ mag}$. Figure 2 (filled triangles) shows K_S magnitude and X-ray flux in the 2–10 keV band for a well-defined subsample of the 2MASS red AGNs observed with *Chandra* (Wilkes et al. 2002). About 20% of them have X-ray flux larger than the detection limit of AMSSn⁵. Therefore, about 3 red AGNs are expected to be detected in our surveys with *ASCA*. This is consistent with our observations that two red AGNs with $K_S < 14 \text{ mag}$ (or four, if errors in the $J - K_S$ color is taken into account) are detected at $z < 0.3$; one is a narrow-line AGN (NO07), and the other is a broad-line AGN (NO10).

5. Summary

We present NIR colors of hard X-ray selected AGNs detected with *ASCA* surveys (ALSS, AMSSn). The flux limit of the sample is $(1 - 3) \times 10^{-13} \text{ erg s}^{-1} \text{ cm}^{-2}$ in the 2–10 keV band in a total surveyed area of $\sim 75 \text{ deg}^2$. Optical follow-up identifications are successful and virtually all the sources were identified. The sample covers the AGNs at $0.1 \lesssim z \lesssim 1$ with $L_{2-10\text{keV}} \sim 10^{42} - 10^{46} \text{ erg s}^{-1}$ with very high completeness. The NIR photometric data of 46 AGNs of the sample are taken from 2MASS Point Source Catalog, 49 AGNs from the observations with KPNO 2.1m telescope, and 9 AGNs from the observations with UH88 inch telescope. The $J - K_S$ color distribution of the *ASCA* AGNs mostly traces that of optically-selected QSOs. The fraction of red ($J - K_S > 2 \text{ mag}$) AGNs in our sample is $\sim 2 \pm 1\%$, which is almost the same as that in optically-selected QSOs. The number of red AGNs found in our sample is consistent with that estimated from the surface density of red AGNs found in 2MASS (Cutri et al. 2001) and the X-ray to K_S flux ratios for the subsample of them (Wilkes et al. 2002). We also found that all QSOs ($L_{2-10 \text{ keV}} \geq 10^{44.5} \text{ erg s}^{-1}$) with a large X-ray absorption ($N_H \geq 10^{22} \text{ cm}^{-2}$) show no or very small absorption in NIR wavelength compared with their X-ray absorption. Estimated dust-to-gas ratios (A_V/N_H) of them are smaller than the Galactic value by about one or two orders of magnitude. Therefore, the anomaly of dust-to-gas ratio in a circumnuclear region of an AGN, which has been shown

⁵Strictly speaking, since the fluxes of the 2MASS red AGNs are simply converted from the Chandra 0.3–8 keV count rate assuming a photon index of 2, the true 2–10 keV fluxes could be significantly larger than the plotted values in Figure 2 if they are heavily absorbed as inferred from their hard spectra (Wilkes et al. 2002). Assuming a typical absorption of $N_H = 10^{22.5} \text{ cm}^{-2}$ at a redshift of 0.2, we expect that about 35% of them have count rates larger than the detection limit of the AMSSn.

for Seyfert-class AGNs by Maiolino et al. (2001), is also seen in QSO-class AGNs. Since a fraction of this population in our sample is about 30% among the sample with the X-ray luminosity larger than $10^{44.5}$ erg s $^{-1}$, such fraction of optical/UV-selected type 1 QSOs known to date may have large amount of dust-less circumnuclear gases.

We would like to thank the staff members of KPNO and UH88 inch telescope. This publication makes use of data products from the Two Micron All Sky Survey, which is a joint project of the University of Massachusetts and the Infrared Processing and Analysis Center, California Institute of Technology, funded by NASA and the National Science Foundation.

REFERENCES

- Akiyama, M. et al. 2000a, ApJ, 532, 700
- Akiyama, M. et al. 2000b, PASJ, 52, 577
- Akiyama, M., & Ohta, K. 2001, PASJ, 53, 63
- Akiyama, M., Ueda, Y., & Ohta, K. 2002, ApJ, 567, 42
- Akiyama, M., Ueda, Y., Ohta, K., Takahashi, T., & Yamada, T. 2003, ApJS, 148, 275
- Barkhouse, W. A., & Hall, P. B. 2001, AJ, 121, 2843
- Cardelli, J. A., Clayton, G. C., & Mathis, J. S. 1989, ApJ, 345, 245
- Coleman, G. D., Wu, C.-C., & Weedman, D. W. 1980. ApJS, 43, 393
- Comastri, A., Fiore, F., Vignalli, C., Matt, G., Perola, G. C., & La Franca, F. 2001. MNRAS, 327, 781
- Cutri, R. M., Nelson, B. O., Kirkpatrick, J. D., Huchra, J. P., & Smith, P. S. 2001, "The New Era of Wide Field Astronomy", ASP Conf. Ser. 232, p78
- Cutri, R. M., Nelson, B. O., Francis, P. J., & Smith, P. S. 2002, "AGN SURVEYS", ASP Conf. Ser. 284, p127
- Elvis, M., et al. 1994, ApJS, 95, 1
- Evans, D. W. 1989, A&AS, 78, 249

- Francis, P. J., Drake, C. L., Whiting, M. T., Drinkwater, M. J., & Webster, R. L. 2001, PASA 18, 221
- Fiore, F., Franca, F. La, Giommi P., Elvis, M., Matt, G., Comastri, A., Molendi, S., & Gioia, I. 2001, MNRAS, 306, L55
- Hasinger, G., et al. 2001, A&A, 365, L45
- Huang, J. S., Glazebrook, K., Cowie, L. L., & Tinney, C. 2003, ApJ, 584, 203
- Irvin, M., Maddox, S., & McMahon, M. Spectrum, 1994, 2, 14
- Kim, D., & Elvis, M. 1999, ApJ, 516, 9
- Loaring, N. S., Page, M. J., & Ramsay, G. 2003, MNRAS, 345, 865
- Maiolino, R., et al. 2001a, A&A, 365, 28
- Maiolino, R., Marconi, A., & Oliva, E. 2001b, A&A, 365, 37
- Percival, W. J., Miller, L., McLure, R. J., & Dunlop, J. S. 2001, MNRAS, 322, 843
- Predehl, P., & Schmitt, J. H. M. M., 1995, A&A, 293, 889
- Risaliti, G., Marconi, A., Maiolino, R., Salvati, M., & Severgnini, P., 2001, A&A, 371, 37
- Risaliti, G., Elvis, M., Gilli, R., & Salvati, M. 2003, ApJ, 587, L9
- Simpson, C. 1998, ApJ, 509, 653
- Smith, P. S., Schmidt, G. D., Hines, D. C., Cutri, R. M., & Nelson, B. O. 2002, ApJ, 569, 23
- Ueda, Y., et al. 1999a, ApJ, 518, 656
- Ueda, Y., Takahashi, T., Ishisaki, Y., Ohashi, T., & Makishima, K. 1999b, ApJ, 524, L11
- Ueda, Y., Ishisaki, Y., Takahashi, T., Makishima, K., & Ohashi, T. 2001, ApJS, 133, 1
- Ueda, Y., Akiyama, M., Ohta, K., & Miyaji, T. 2003, ApJ, 598, 886
- Veron-Cetty, M. P., & Veron, P., 2000, ESO Sci. Rep., 19, 1
- Vignali, C., Mignoli, M., Comastri, A., Maiolino, R., & Fiore, F. 2000, MNRAS, 314, 11
- Wainscoat, R. J., & Cowie, L. L. 1992, AJ, 103, 332

- Webster, R. L., Francis, P. J., Peterson, B. A., Drinkwater, M. J., & Masci, F. J. 1995, *Nature*, 375, 469
- Weingartner, J. C., & Murray, N. 2002, *ApJ*, 580, 88
- White, R. L., Helfand, D. J., Becker, R. H., Gregg, M. D., Postman, M., Lauer, T. R., & Oegerle, W. 2003, *AJ*, 126, 706
- Wilkes, B. J., Schmidt, G. D., Cutri, R. M., Ghosh, H., Hines, D. C., Nelson, B., & Smith, P. S. 2002, *ApJ*, 564L, 65
- Willott, C. J. et al. 2003, *MNRAS*, 339, 397

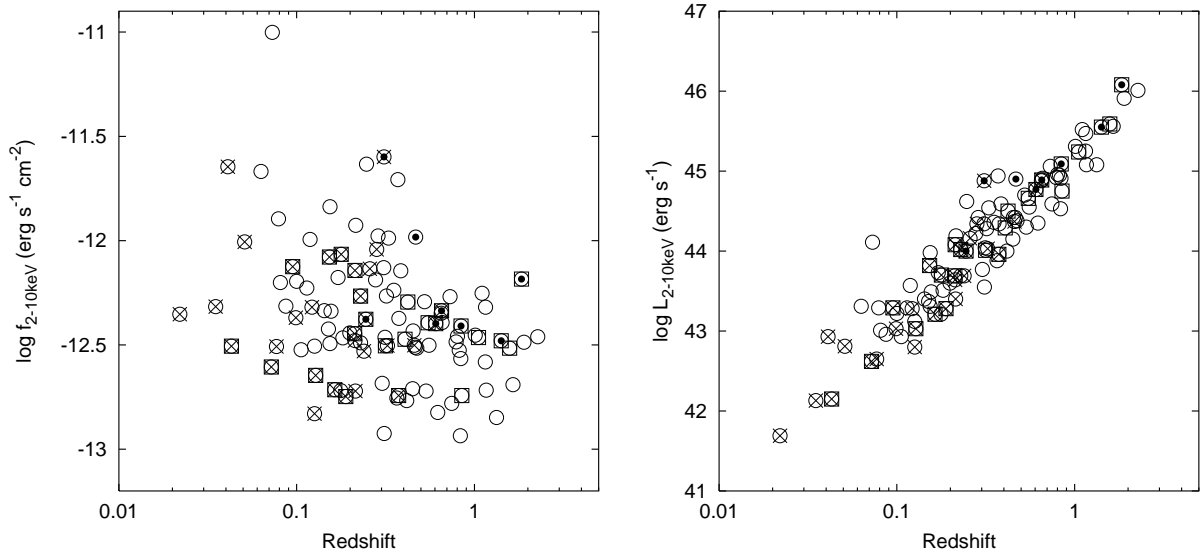


Fig. 1.— *Left*: 2–10 keV flux against redshift for the *ASCA* AGNs. Over-plotted filled circles, crosses, and open squares indicate AGNs with a large hard X-ray to optical flux ratio (optically faint; $\log f_{2-10 \text{ keV}}/f_R > 1$), AGNs showing no significant broad $\text{H}\beta$ emission line, and AGNs with large X-ray absorption ($N_{\text{H}} \geq 10^{22} \text{ cm}^{-2}$), respectively.

Right: Absorption corrected X-ray luminosity in the rest-frame 2–10 keV band against redshift for the *ASCA* AGNs.

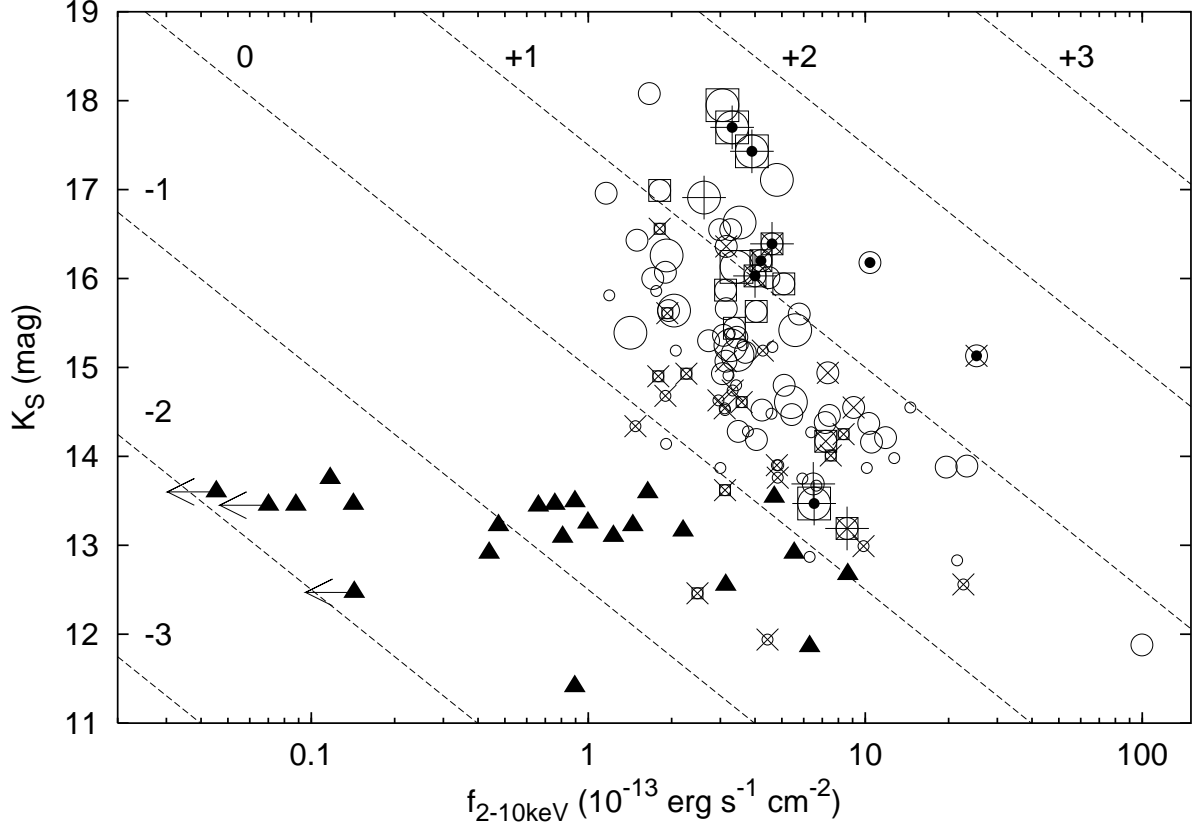


Fig. 2.— K_S magnitude against 2–10 keV X-ray flux for *ASCA* AGNs (open circles). Symbol sizes represent the absorption corrected rest-frame luminosity in the 2–10 keV band; large, middle, and small symbols represent AGNs with $L_{2-10 \text{ keV}} > 10^{45} \text{ erg s}^{-1}$, $10^{44-45} \text{ erg s}^{-1}$, and $< 10^{44} \text{ erg s}^{-1}$, respectively. Over-plotted filled circles, crosses, and open squares are the same as those in Figure 1. Over-plotted pluses indicate the red AGNs; two AGNs with $J - K_S > 2 \text{ mag}$ and six AGNs with $J - K_S \sim 2 \text{ mag}$ at $z > 0.6$, which are described in Section 4.3. Filled triangles show the 2MASS red ($J - K_S > 2 \text{ mag}$) AGNs (Smith et al. 2002, Wilkes et al. 2002). Dashed lines represent the constant X-ray to NIR flux ratio of $\log f_{2-10 \text{ keV}}/f_{K_S} = +3, +2, +1, 0, -1, -2$, and -3 from top to bottom.

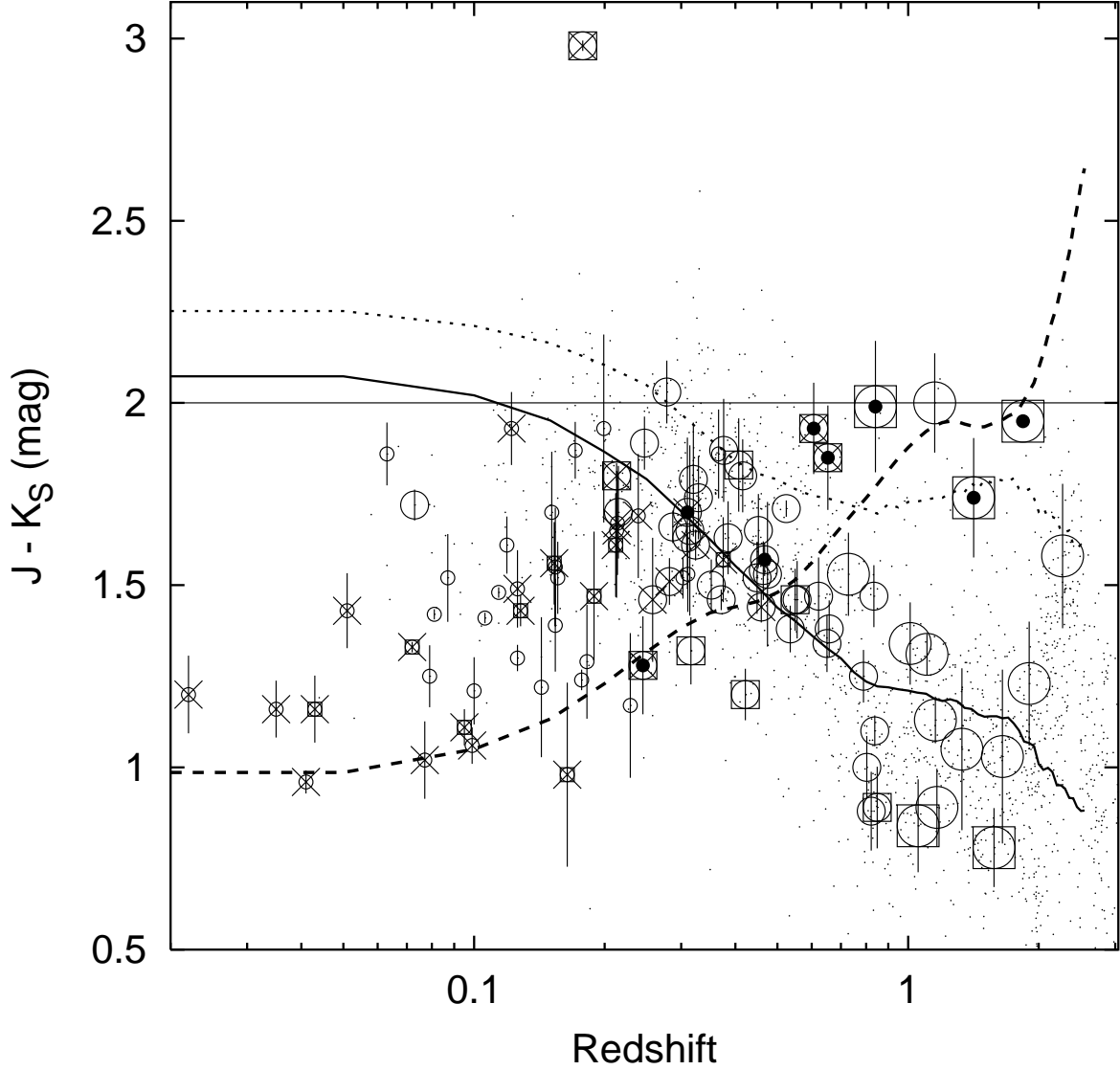


Fig. 3.— $J - K_S$ color vs redshift for the *ASCA* AGNs (open circles). Over-plotted filled circles, crosses, and open squares are the same as those in Figure 1. Small dots indicate color distribution of optically-selected QSOs measured in the 2MASS survey (Barkhouse & Hall 2001). $J - K_S$ color track for the mean-QSO spectrum by Elvis et al. (1994), that for the same mean-QSO spectrum with absorption with $A_V = 1$ mag, and that for an Sbc galaxy taken from Coleman et al. (1980) are shown with solid, dotted, and dashed lines, respectively. No spectral evolution is considered.

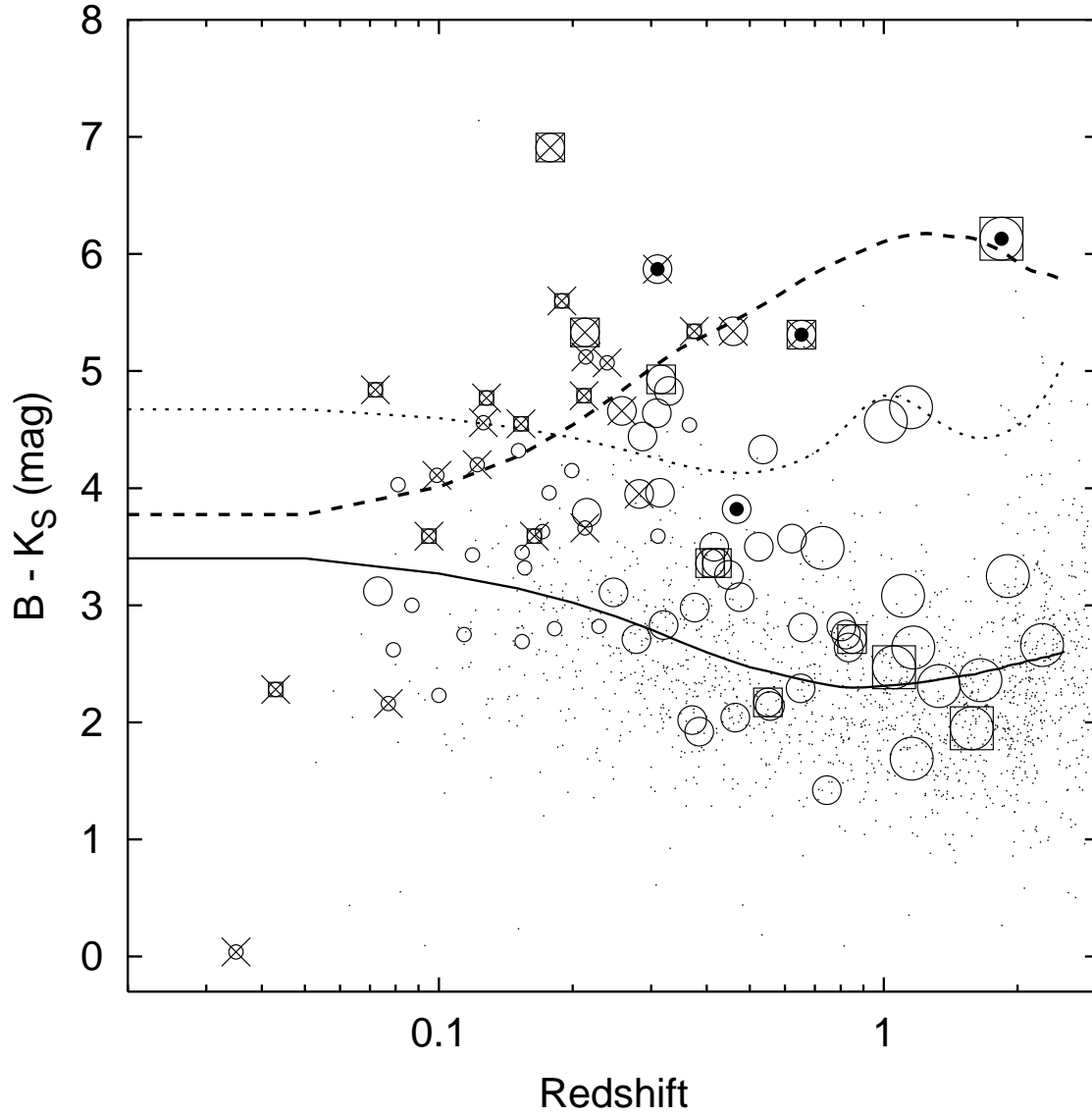


Fig. 4.— Same as figure 3, but for $B - K_S$ color.

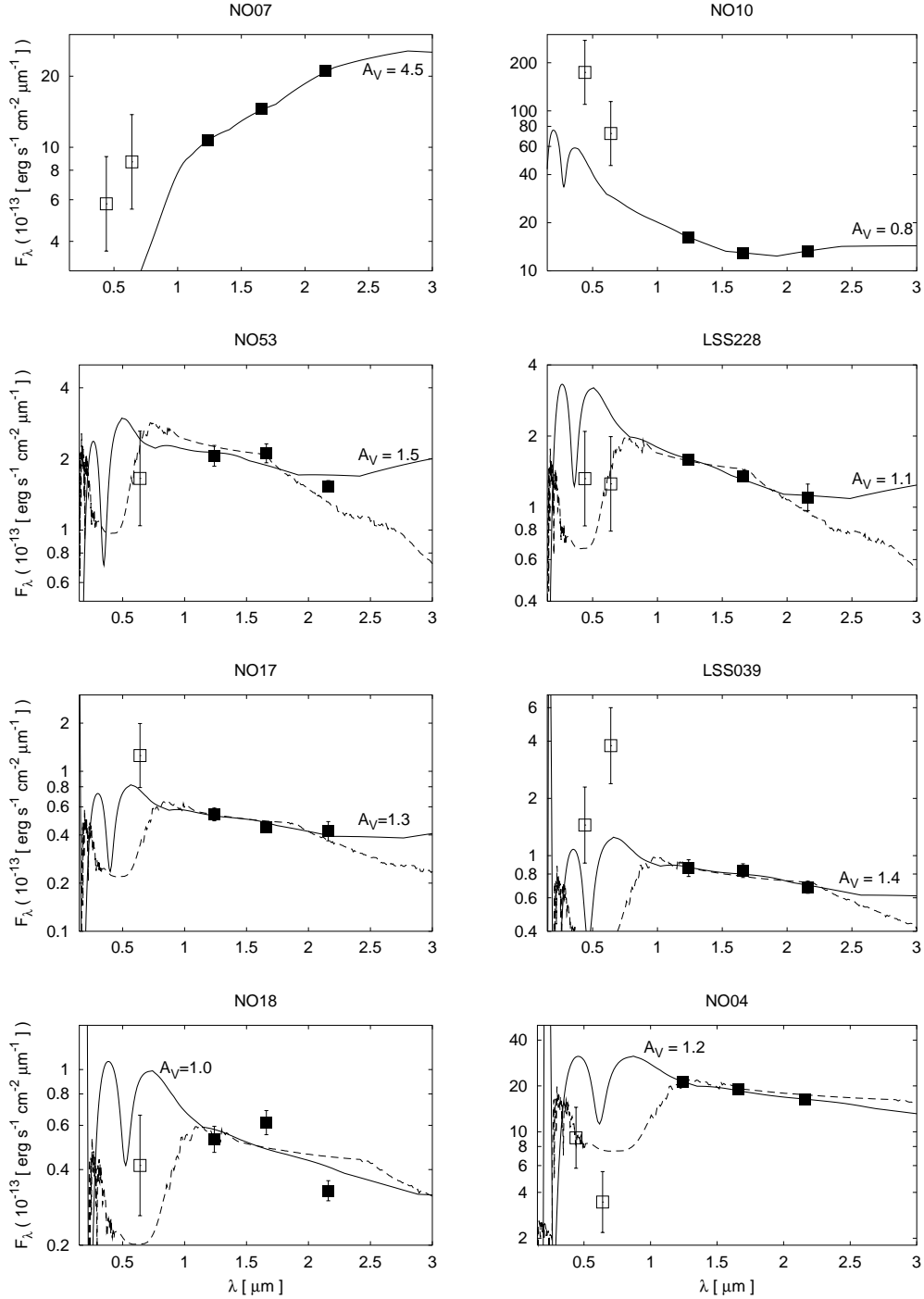


Fig. 5.— Spectral energy distributions of the red AGNs in the sample; two AGNs with $J - K_S > 2$ mag (NO07, NO10) and six AGNs with $J - K_S \sim 2$ mag at $z > 0.6$ (NO53, LSS228, NO17, LSS039, NO18, NO04), which are described in Section 4.3. Filled and open squares show the photometric data of NIR (J , H , K_S) and optical (B , R) bands, respectively. Solid lines indicate the best-fit reddened QSO spectrum (in detail see section 4.3) with A_V shown in the panels. Dashed lines show the best-fit Sbc-galaxy template spectrum by Coleman et al.(1980) without absorption. Errors on B and R magnitudes are taken to be 0.5 mag.

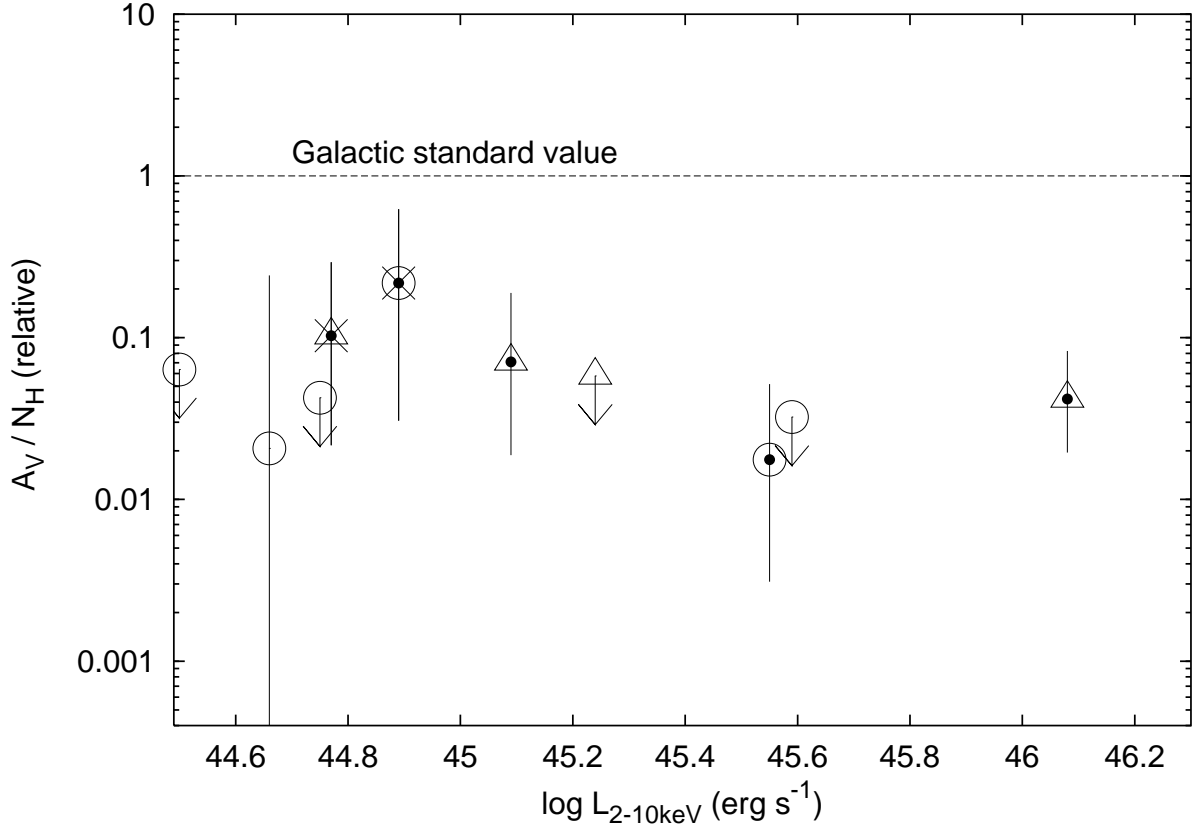


Fig. 6.— A_V/N_H value normalized by the Galactic value of 5.6×10^{-22} mag cm² against absorption corrected X-ray luminosity in the rest-frame 2–10 keV band for the sample objects with $N_H \geq 10^{22}$ cm⁻² and $L_{2-10 \text{ keV}} \geq 10^{44.5}$ erg s⁻¹. Open circles and open triangles refer to the radio-quiet and radio-loud QSOs, respectively. Over-plotted filled circles and crosses are the same as in Figure 1. Arrows show upper limits of A_V/N_H value. The N_H is estimated from the X-ray spectrum with an assumption of an intrinsic power-law photon index of 1.9, and A_V is calculated from the observed $J - K_S$ color by assuming that the intrinsic spectrum of a QSO is the same as that of the mean-QSO spectrum by Elvis et al. (1994).

Table 1. Properties of *ASCA* AGNs

Name ^a	<i>J</i>	<i>H</i>	<i>K_S</i>	<i>J</i> − <i>K_S</i>	<i>B</i> ^b	<i>R</i> ^b	NIR Data ^c Source	<i>z</i> ^d	flux ^e 2−10keV	log <i>L</i> ^f 2−10keV	<i>N_H</i> ^g	Γ ^h
	(mag)	(mag)	(mag)	(mag)	(mag)	(mag)						
1AXG J000605+2031 NE01	16.01±0.08	15.59±0.13	14.38±0.06	1.63	16.3	16.2	2MASS	0.385	7.17	44.59	0	2.2 ^{+0.3} _{−0.2}
1AXG J000927−0438 NO19	16.99±0.17	16.08±0.17	15.34±0.16	1.65	19.3	18.3	2MASS	0.314	3.44	44.04	0	2.1 ^{+0.2} _{−0.2}
1AXG J001913+1556 NE18	16.72±0.14	15.81±0.13	15.14±0.14	1.58	17.8	17.5	2MASS	2.270	3.46	46.01	0	1.9 ^{+0.2} _{−0.2}
1AXG J002619+1050 NO49	16.46±0.13	15.88±0.18	14.93±0.15	1.53	18.0	17.5	2MASS	0.474	3.05	44.38	0.37 ^{+0.38} _{−0.35}	1.9
1AXG J002637+1725 NO50	14.78±0.07	14.11±0.09	13.62±0.06	1.16	15.9	14.4	2MASS	0.043	3.12	42.15	1.34 ^{+0.44} _{−0.36}	1.9
1AXG J015840+0347 NO46	15.57±0.05	15.08±0.09	14.19±0.06	1.38	17.0	16.8	2MASS	0.658	4.05	44.91	0	2.3 ^{+0.2} _{−0.2}
1AXG J023520−0347 NO16	16.39±0.10	15.44±0.11	14.52±0.10	1.87	17.5	17.4	2MASS	0.376	4.24	44.34	0	2.3 ^{+0.2} _{−0.1}
1AXG J033516−1505 SE20	15.83±0.08	14.95±0.09	13.90±0.06	1.92	18.1	16.5	2MASS	0.122	4.80	43.28	0.58 ^{+0.19} _{−0.18}	1.9
1AXG J035137−1204 SE17	16.09±0.10	15.33±0.10	14.80±0.12	1.29	17.6	17.1	2MASS	0.182	3.42	43.51	0.80 ^{+0.40} _{−0.35}	1.9
1AXG J041757+0101 NE25	15.82±0.03	15.32±0.04	14.52±0.02	1.30	...	17.0 ^S	KPNO	0.126	3.12	43.12	0.43 ^{+0.39} _{−0.32}	1.9
1AXG J043420−0822 NE03	15.94±0.09	15.28±0.10	14.55±0.09	1.39	18.0	17.9	2MASS	0.154	14.55	43.98	0.71 ^{+0.19} _{−0.16}	1.9
1AXG J044749−0629 NO08	16.39±0.14	15.36±0.14	14.74±0.12	1.66	18.4	17.7	2MASS	0.213	3.32	43.64	0.31 ^{+0.24} _{−0.22}	1.9
1AXG J083747+6513 NO06	16.73±0.04	16.29±0.07	15.42±0.04	1.31	18.5	18.1	KPNO	1.105	5.59	45.52	0	2.0 ^{+0.1} _{−0.1}
1AXG J090053+3856 NO54	16.72±0.15	16.09±0.21	>15.28	1.44	20.8 ^U	18.2 ^U	2MASS	0.229	5.42	44.02	5.23 ^{+1.92} _{−1.29}	1.9
1AXG J102337+1936 NE12	17.27±0.10	16.61±0.13	15.44±0.08	1.83	18.8	18.0	KPNO	0.407	3.37	44.29	1.31 ^{+0.76} _{−0.64}	1.9
1AXG J103934+5330 NO11	16.55±0.13	15.91±0.17	15.38±0.15	1.17	18.2	17.6	2MASS	0.229	3.24	43.69	0.10 ^{+0.26} _{−0.10}	1.9
1AXG J104026+2046 NO41	17.75±0.02	16.87±0.05	16.18±0.04	1.57	20.0 ^U	19.5 ^U	UH	0.467	10.40	44.90	0.12 ^{+0.15} _{−0.12}	1.9
1AXG J105722−0351 NE14	17.12±0.08	16.58±0.14	15.66±0.07	1.46	17.8	17.8	KPNO	0.555	3.15	44.55	0.41 ^{+0.62} _{−0.41}	1.9
1AXG J111432+4055 NE26	15.81±0.08	15.14±0.08	14.25±0.08	1.56	18.8	16.4	2MASS	0.153	8.35	43.82	4.10 ^{+1.37} _{−0.98}	1.9
1AXG J111518+4042 NO56	15.23±0.06	14.51±0.07	13.98±0.06	1.25	16.6	15.1	2MASS	0.079	12.73	43.29	0	2.0 ^{+0.0} _{−0.0}
1AXG J121328+2938 NO28	16.45±0.12	15.68±0.13	15.23±0.15	1.22	...	16.8 ^S	2MASS	0.143	4.62	43.40	0	1.9 ^{+0.1} _{−0.1}
1AXG J121359+1404 NO01	16.46±0.11	15.67±0.13	14.91±0.12	1.55	17.6	17.0	2MASS	0.154	3.21	43.31	0.06 ^{+0.22} _{−0.06}	1.9
1AXG J121427+2936 NO27	16.09±0.03	15.38±0.04	14.46±0.02	1.63	19.1	17.5	KPNO	0.309	7.42	44.34	0.29 ^{+0.16} _{−0.15}	1.9
1AXG J121854+2957 NO07	16.17±0.01	14.73±0.01	13.19±0.01	2.98	20.1 ^U	18.5 ^U	UH	0.178	8.6 ⁱ	44.04 ⁱ	8.2 ^{+1.1} _{−0.7}	2.0 ^{+0.2} _{−0.2}
1AXG J121930+0643 NO44	14.29±0.01	13.62±0.02	12.87±0.01	1.42	16.9	16.0	KPNO	0.081	6.30	43.01	0	2.2 ^{+0.1} _{−0.1}
1AXG J121930+7532 NO39	16.90±0.07	16.10±0.08	15.36±0.04	1.54	17.4	17.2	KPNO	0.464	3.08	44.42	0	2.3 ^{+0.2} _{−0.2}
1AXG J122003−0025 NO03	17.14±0.05	16.64±0.09	15.94±0.05	1.20	19.3	18.9	KPNO	0.422	5.08	44.50	1.12 ^{+0.49} _{−0.43}	1.9
1AXG J122017+0641 NO45	15.82±0.04	15.10±0.04	14.16±0.02	1.66	18.6 ^S	17.7 ^S	KPNO	0.287	10.53	44.42	0	1.9 ^{+0.1} _{−0.1}
1AXG J122049+7505 NO37	17.35±0.05	16.69±0.07	16.01±0.06	1.34	18.3	17.7	KPNO	0.650	4.49	44.88	0	2.0 ^{+0.2} _{−0.2}

Table 1—Continued

Name ^a	J	H	K_S	$J-K_S$	B^b	R^b	NIR Data ^c Source	z^d	flux ^e 2–10keV	$\log L^f$ 2–10keV	N_H^g	Γ^h
	(mag)	(mag)	(mag)	(mag)	(mag)	(mag)						
1AXG J122135+7518 NO38	13.60±0.03	12.68±0.03	11.88±0.03	1.72	15.0	13.9	2MASS	0.073	99.70	44.11	0	2.0 ^{+0.0} _{-0.0}
1AXG J122155+7525 NO40	16.32±0.13	15.42±0.12	14.63±0.11	1.69	19.7 ^U	17.4 ^U	2MASS	0.239	2.95	43.69	0.26 ^{+0.31} _{-0.26}	1.9
1AXG J123605+2613 NE04	17.80±0.03	17.00±0.04	16.36±0.03	1.44	21.7	19.5 ^S	KPNO	0.459	3.15	44.37	0.78 ^{+0.71} _{-0.61}	1.9
1AXG J125732+3543 NO31	16.51±0.02	15.63±0.02	14.80±0.01	1.71	18.3	18.0	UH	0.524	5.10	44.70	0.07 ^{+0.27} _{-0.07}	1.9
1AXG J125812+3519 NE16	16.83±0.15	15.92±0.15	15.13±0.14	1.71	21.0	18.5	2MASS	0.310	25.22	44.88	0.14 ^{+0.15} _{-0.14}	1.9
1AXG J125828+3528 NE15	16.48±0.11	15.79±0.14	15.25±0.13	1.23	18.5	17.4	2MASS	1.900	3.26	45.91	0	2.1 ^{+0.2} _{-0.2}
1AXG J130407+3533 NO30	16.11±0.09	15.37±0.10	14.37±0.07	1.74	19.2	17.6	2MASS	0.329	10.29	44.54	0.15 ^{+0.11} _{-0.11}	1.9
1AXG J130453+3548 NO29	17.19±0.07	16.93±0.11	15.87±0.06	1.32	20.8	18.9	KPNO	0.316	3.13	44.01	1.28 ^{+0.74} _{-0.62}	1.9
1AXG J132310–1656 SE34	13.14±0.08	12.29±0.09	11.94±0.07	1.20	...	15.0 ^S	2MASS	0.022	4.44	41.69	0.19 ^{+0.25} _{-0.19}	1.9
1AXG J134412+0016 NE20	16.82±0.08	15.95±0.09	15.17±0.06	1.65	...	19.0	KPNO	0.452	3.69	44.42	0.56 ^{+0.56} _{-0.49}	1.9
1AXG J134450+0005 NE19	15.42±0.08	14.57±0.09	13.90±0.09	1.53	16.9	15.6	2MASS	0.087	4.85	42.96	0	2.2 ^{+0.1} _{-0.1}
1AXG J134741–1122 SE30	15.48±0.07	14.72±0.04	14.27±0.06	1.21	16.5	17.2	KPNO	0.100	6.38	43.22	0.47 ^{+0.37} _{-0.32}	1.9
1AXG J140528+2224 NO15	16.00±0.07	15.28±0.09	14.48±0.07	1.43	17.8	16.5	2MASS	0.156	4.59	43.49	0	2.1 ^{+0.1} _{-0.1}
1AXG J140532+5055 NO13	15.28±0.01	14.48±0.02	13.87±0.01	1.41	...	17.8 ^S	KPNO	0.106	3.00	42.93	0	2.0 ^{+0.2} _{-0.2}
1AXG J141240–1209 SE03	15.78±0.07	14.90±0.07	13.89±0.02	1.89	17.0	16.7	KPNO	0.247	23.26	44.62	0.13 ^{+0.07} _{-0.06}	1.9
1AXG J141426–1209 SE28	18.24±0.04	17.58±0.04	17.11±0.05	1.13	18.8	18.4	UH	1.156	4.80	45.47	0	1.9 ^{+0.2} _{-0.2}
1AXG J142353+2247 NE09	16.06±0.04	15.28±0.05	14.55±0.05	1.51	18.5	16.8	KPNO	0.282	9.08	44.34	0.10 ^{+0.18} _{-0.10}	1.9
1AXG J142651+2619 NO51	16.40±0.13	15.54±0.12	14.94±0.11	1.46	19.6	17.6	2MASS	0.258	7.33	44.16	0	1.9 ^{+0.1} _{-0.1}
1AXG J144055+5204 NE13	16.26±0.12	15.77±0.16	14.47±0.10	1.79	17.3	16.7	2MASS	0.320	5.43	44.28	0	2.3 ^{+0.2} _{-0.2}
1AXG J144109+3520 NO32	15.56±0.07	14.90±0.10	14.54±0.08	1.02	16.7	15.8	2MASS	0.077	3.11	42.65	0	2.0 ^{+0.2} _{-0.2}
1AXG J144301+5208 NO26	16.22±0.11	15.61±0.16	14.61±0.09	1.61	19.4	17.2	2MASS	0.212	3.58	43.69	1.32 ^{+0.41} _{-0.34}	1.9
1AXG J150339+1016 NO05	15.12±0.03	14.45±0.04	14.01±0.04	1.11	17.6	16.1	KPNO	0.095	7.51	43.29	1.95 ^{+0.27} _{-0.26}	1.9
1AXG J150423+1029 NO04	15.42±0.01	14.44±0.01	13.47±0.01	1.95	19.6	19.5	KPNO	1.839	6.54	46.08	5.41 ^{+1.82} _{-1.65}	1.9
1AXG J150430+4741 NO12	17.43±0.06	17.20±0.10	16.55±0.09	0.88	19.3	18.5	KPNO	0.822	2.98	44.95	0	2.0 ^{+0.1} _{-0.1}
1AXG J151441+3650 NE10	15.34±0.02	14.63±0.04	13.88±0.02	1.46	15.9	15.8	KPNO	0.371	19.61	44.94	0.11 ^{+0.16} _{-0.11}	1.9
1AXG J151524+3639 NO21	16.68±0.03	15.83±0.04	15.07±0.03	1.61	...	18.5	KPNO	0.324	3.14	44.03	0.90 ^{+0.55} _{-0.49}	1.9
1AXG J155810+6401 NO22	17.10±0.05	16.38±0.06	15.60±0.05	1.50	...	19.1	KPNO	0.352	5.78	44.36	0.15 ^{+0.21} _{-0.15}	1.9
1AXG J160118+0844 NO53	17.96±0.11	16.83±0.10	16.03±0.06	1.93	...	20.3 ^S	KPNO	0.606	4.00	44.77	2.95 ^{+1.58} _{-1.23}	1.9
1AXG J163538+3809 NO47	16.25±0.03	15.54±0.03	15.19±0.04	1.06	19.3	17.5	KPNO	0.099	4.27	43.03	0.38 ^{+0.17} _{-0.15}	1.9

Table 1—Continued

Name ^a	J	H	K_S	$J-K_S$	B^b	R^b	NIR Data ^c Source	z^d	flux ^e 2–10keV	$\log L^f$ 2–10keV	N_H^g	Γ^h
	(mag)	(mag)	(mag)	(mag)	(mag)	(mag)						
1AXG J163720+8207 NE08	13.52±0.01	12.89±0.02	12.56±0.03	0.96	...	16.0 ^S	KPNO	0.041	22.62	42.93	0.20 ^{+0.11} _{-0.11}	1.9
1AXG J170305+4526 NO35	15.54±0.06	14.69±0.07	13.67±0.05	1.88	17.3	16.8	2MASS	0.171	6.66	43.73	0.26 ^{+0.15} _{-0.14}	1.9
1AXG J170548+2412 NE11	15.23±0.01	14.41±0.01	13.75±0.01	1.48	16.5 ^U	14.5 ^U	KPNO	0.114	5.93	43.29	0.00 ^{+0.26} _{-0.00}	1.9
1AXG J170730+2353 NO24	17.48±0.09	17.05±0.11	16.20±0.10	1.28	...	20.0	KPNO	0.245	4.20	44.00	7.07 ^{+41.91} _{-2.90}	1.9
1AXG J171125+7111 NO02	17.97±0.08	17.42±0.09	16.63±0.08	1.34	21.2	18.5 ^S	KPNO	1.011	3.52	45.31	0	2.2 ^{+0.1} _{-0.1}
1AXG J171811+6727 NE21	17.09±0.06	16.40±0.05	15.63±0.06	1.46	17.8	17.7	KPNO	0.549	4.04	44.66	1.51 ^{+0.60} _{-0.55}	1.9
1AXG J172938+5230 NO10	15.72±0.07	14.86±0.06	13.69±0.05	2.03	16.4	16.2	2MASS	0.278	6.49	44.22	0	2.3 ^{+0.1} _{-0.1}
1AXG J174652+6836 NO42	14.69±0.07	13.84±0.08	12.83±0.05	1.86	...	16.0 ^S	2MASS	0.063	21.46	43.31	0	2.0 ^{+0.0} _{-0.0}
1AXG J174943+6823 NO43	14.42±0.09	13.53±0.08	12.99±0.05	1.43	...	16.0 ^S	2MASS	0.051	9.86	42.81	0.75 ^{+0.18} _{-0.18}	1.9
1AXG J210738–0512 NO17	19.42±0.10	18.52±0.08	17.43±0.15	1.99	...	20.6 ^S	UH	0.841	3.90	45.09	4.27 ^{+2.10} _{-1.67}	1.9
1AXG J230738–1526 SE14	17.18±0.21	16.14±0.21	15.25±0.15	1.93	19.4	18.3	2MASS	0.199	3.61	43.60	0.03 ^{+0.24} _{-0.03}	1.9
1AXG J232639+2205 NO48	15.98±0.14	15.32±0.11	14.28±0.09	1.70	18.6 ^U	17.2 ^U	2MASS	0.151	3.77	43.37	0.31 ^{+0.34} _{-0.31}	1.9
1AXG J233200+1945 NO18	19.44±0.13	18.17±0.12	17.70±0.10	1.74	...	21.8 ^U	UH	1.416	3.31	45.55	10.86 ^{+6.25} _{-4.52}	1.9
1AXG J233253+1513 NO14	15.91±0.09	15.14±0.09	14.21±0.09	1.70	18.0	16.6	2MASS	0.215	11.84	44.19	0	1.9 ^{+0.1} _{-0.1}
1AXG J234725+0053 NE23	15.97±0.01	15.20±0.01	14.17±0.01	1.80	19.5	17.5	UH	0.213	7.20	44.08	1.42 ^{+0.43} _{-0.35}	1.9
1AXG J235554+2836 NO20	16.14±0.09	15.73±0.14	14.61±0.07	1.53	18.1	17.7	2MASS	0.729	5.39	45.06	0.73 ^{+0.57} _{-0.53}	1.9
AX J130826+3005 LSS023	15.28±0.05	15.17±0.08	14.28±0.07	1.00	17.1	16.3	2MASS	0.803	3.48	44.96	0	1.9 ^{+0.2} _{-0.2}
AX J130840+2955 LSS014	16.59±0.14	15.93±0.16	15.61±0.21	0.98	19.2	17.3	2MASS	0.164	1.93	43.21	2.64 ^{+1.27} _{-1.27}	1.9
AX J130926+2952 LSS016	18.13±0.10	17.13±0.06	16.56±0.06	1.57	21.9 ^U	19.9 ^U	KPNO	0.375	1.81	43.96	2.82 ^{+1.90} _{-1.25}	1.9
AX J131015+3004 LSS033	17.15±0.07	16.49±0.10	16.26±0.08	0.89	18.9	17.9	KPNO	1.165	1.92	45.08	0.00 ^{+1.92} _{-0.00}	1.9
AX J131021+3019 LSS039	18.91±0.11	17.84±0.09	16.91±0.08	2.00	21.6 ^U	19.4 ^K	KPNO	1.152 ^j	2.62 ^k	45.25 ^k	0.00 ^{+0.02} _{-0.00}	2.0 ^{+0.1k} _{-0.1}
AX J131054+3004 LSS037	18.73±0.06	...	17.95±0.09	0.78	19.9	19.2	UH	1.577	3.05	45.59	2.48 ^{+1.71} _{-1.71}	1.9
AX J131128+3105 LSS080	16.44±0.13	16.24±0.23	15.39±0.18	1.04	17.7	17.1	2MASS	1.331	1.42	45.08	0.00 ^{+2.88} _{-0.00}	1.9
AX J131156+3054 LSS075	17.72±0.10	16.97±0.11	15.86±0.07	1.86	20.4	19.2	KPNO	0.366	1.76	43.88	0.00 ^{+0.83} _{-0.00}	1.9
AX J131210+3048 LSS072	16.37±0.13	>15.36	14.90±0.12	1.47	20.5 ^U	18.4 ^U	2MASS	0.189	1.79	43.28	1.42 ^{+0.99} _{-0.70}	1.9
AX J131249+3112 LSS096	16.97±0.09	17.01±0.21	16.13±0.09	0.83	18.6	17.9	KPNO	1.055	3.43	45.24	1.00 ^{+0.60} _{-0.60}	1.9
AX J131321+3119 LSS103	18.43±0.06	17.86±0.08	16.96±0.06	1.47	19.6	19.8	KPNO	0.834	1.16	44.53	0.92 ^{+0.65} _{-0.65}	1.9
AX J131327+3155 LSS121	16.71±0.04	15.83±0.07	15.19±0.04	1.52	...	17.6 ^K	KPNO	0.303	2.07	43.77	0.16 ^{+0.24} _{-0.16}	1.9
AX J131345+3118 LSS104	17.80±0.04	17.35±0.10	16.55±0.06	1.25	...	19.3 ^K	KPNO	0.789	3.27	44.92	0.16 ^{+0.39} _{-0.16}	1.9

Table 1—Continued

Name ^a	<i>J</i>	<i>H</i>	<i>K_S</i>	<i>J−K_S</i>	<i>B</i> ^b	<i>R</i> ^b	NIR Data ^c Source	<i>z</i> ^d	flux ^e 2–10keV	log <i>L</i> ^f 2–10keV	<i>N_H</i> ^g	Γ ^h
	(mag)	(mag)	(mag)	(mag)	(mag)	(mag)						
AX J131407+3158 LSS127	15.38±0.02	14.81±0.03	14.14±0.02	1.24	18.1	16.7	KPNO	0.177	1.91	43.21	0.07 ^{+0.27} _{−0.07}	1.9
AX J131501+3141 LSS119	13.79±0.01	12.95±0.01	12.46±0.01	1.33	17.3 ^U	15.6 ^U	KPNO	0.072	2.48 ^l	42.62 ^l	6.40 ^{+1.90} _{−1.40}	1.5 ^{+0.41} _{−0.4}
AX J131521+3159 LSS136	16.40±0.03	16.00±0.03	15.30±0.03	1.10	...	17.7 ^B	KPNO	0.838	2.72	44.91	0	1.9 ^{+0.2} _{−0.2}
AX J131529+3117 LSS110	17.16±0.07	16.43±0.12	15.64±0.07	1.52	18.9	18.8	KPNO	0.449	1.95	44.15	0	2.0 ^{+0.2} _{−0.2}
AX J131551+3237 LSS171	16.36±0.03	15.67±0.04	14.93±0.03	1.43	19.7 ^U	18.1 ^U	KPNO	0.128	2.26 ^l	43.03 ^l	1.90 ^{+0.80} _{−0.60}	1.9 ^{+0.41} _{−0.4}
AX J131639+3149 LSS137	17.90±0.08	17.22±0.11	16.43±0.07	1.47	20.0	20.0	KPNO	0.622	1.50	44.35	0.35 ^{+0.49} _{−0.35}	1.9
AX J131707+3237 LSS175	18.38±0.12	18.21±0.22	18.08±0.94	0.30	19.5	18.6	KPNO	0.745	1.66	44.59	0	2.0 ^{+0.2} _{−0.2}
AX J131724+3203 LSS152	17.88±0.05	17.61±0.07	16.99±0.10	0.89	19.7	19.1	KPNO	0.849	1.81	44.75	1.90 ^{+0.99} _{−0.99}	1.9
AX J131725+3300 LSS192	15.83±0.08	14.98±0.09	14.34±0.07	1.49	18.9	16.6	2MASS	0.126	1.48	42.80	0.42 ^{+0.24} _{−0.24}	1.9
AX J131758+3257 LSS195	16.35±0.11	15.49±0.09	14.68±0.09	1.67	19.8 ^U	18.0 ^U	2MASS	0.214	1.90	43.40	0.28 ^{+0.19} _{−0.19}	1.9
AX J131805+3349 LSS233	14.92±0.06	14.24±0.07	13.76±0.05	1.16	13.8	13.4	2MASS	0.035	4.83	42.13	0.28 ^{+0.17} _{−0.17}	1.9
AX J131816+3240 LSS183	16.67±0.13	16.00±0.14	15.64±0.20	1.03	18.0 ^U	17.5 ^U	2MASS	1.649	2.04 ^k	45.56 ^k	0.00 ^{+0.08} _{−0.00}	2.1 ^{+0.1} _{−0.1}
AX J131822+3347 LSS235	15.48±0.06	14.73±0.07	13.87±0.05	1.61	17.3	16.4	2MASS	0.119	10.14	43.57	0	2.0 ^{+0.1} _{−0.1}
AX J131831+3320 LSS212	17.45±0.04	16.66±0.05	16.07±0.05	1.38	20.4	19.7	KPNO	0.535	1.90	44.30	0.36 ^{+0.24} _{−0.24}	1.9
AX J131831+3341 LSS228	18.24±0.03	17.32±0.03	16.39±0.14 ^m	1.86	21.7 ^U	20.6 ^U	UH	0.653	4.61	44.89	1.14 ^{+0.43} _{−0.43}	1.9
AX J131927+3343 LSS238	17.80±0.08	16.78±0.08	16.00±0.06	1.80	19.5 ^U	18.9 ^U	KPNO	0.416	1.71	44.00	0.64 ^{+0.43} _{−0.43}	1.9
AX J131928+3251 LSS197	17.34±0.09	16.67±0.10	15.81±0.05	1.53	19.4	18.4	KPNO	0.311	1.19	43.55	0.28 ^{+0.37} _{−0.28}	1.9

^aX-ray source name and identification number (Ueda et al. 1999, 2001, Akiyama et al. 2000a, 2003).

^bB and R magnitudes from APM catalog, unless otherwise noted. Magnitudes are converted from O and E magnitudes of APM catalogue by using the equations by Evans (1989). U : Determined by photometric observations with a CCD camera on the UH88 inch telescope (Akiyama et al. 2003). S : Determined from the spectrophotometric data (Akiyama et al. 2003). K : Determined by relative photometry with mosaic CCD image taken at KISO observatory (Akiyama et al. 2000a). B : APM magnitude data is blended. Deblending was done using CCD image taken during the spectroscopic observations (Akiyama et al. 2000a).

^cKPNO, 2MASS, and UH shows Kitt Peak National Observatory (2.1m telescope), 2MASS All-Sky Point Source Catalog, and University of Hawaii (88 inch telescope), respectively.

^dRedshift determined by the spectroscopic observations in optical (Akiyama et al. 2000a, 2003).

^e2–10keV flux in units of 10^{-13} erg s^{−1} cm^{−2}. Conversions from countrates are done based on the best-fit absorbed power-law spectra. (More details for the conversions

are described by Ueda et al. 2003).

^fAbsorption-corrected luminosity in the rest-frame 2–10keV band in units of erg s^{-1} .

^gBest fit rest-frame hydrogen column density for the absorbed power-law model in units of 10^{22} cm^{-2} . The value of 0 without error indicates that $N_{\text{H}} = 0$ is assumed if the best-fit photon index is larger than 1.9. See Section 2 and Ueda et al. (2003) for the details.

^hIntrinsic photon index. The value of 1.9 without error indicates that the intrinsic photon index of 1.9 is assumed if the best-fit photon index is smaller than 1.9. See Section 2 and Ueda et al. (2003) for the details.

ⁱX-ray data from Loaring et al.(2003).

^jThe identification of this X-ray source was not correct in Akiyama et al. (2000a). See the footnote in section 4.3.2.

^kX-ray data from the follow-up observation with *XMM-Newton*. See Ueda et al. (2003).

^lX-ray data from the follow-up observation with *ASCA*.

^m K_S magnitude converted from K magnitude by Akiyama and Ohta (2001).